Fermi surface and band renormalization of $Sr_{1-x}K_xFe_2As_2$ from angle-resolved photoemission spectroscopy

Haiyun Liu,[1] Wentao Zhang,[1] Lin Zhao,[1] Xiaowen Jia,[1] Jianqiao Meng,[1] Guodong Liu,[1] Xiaoli Dong,[1] G. F. Chen,[2] J. L. Luo,[2] N. L. Wang,[2] Wei Lu,[1] Guiling Wang,[3] Yong Zhou,[3] Yong Zhu,[4] Xiaoyang Wang,[4] Zuyan Xu,[3] Chuangtian Chen,[4] and X. J. Zhou[1,*]

[1]*National Laboratory for Superconductivity, Beijing National Laboratory for Condensed Matter Physics, Institute of Physics, Chinese Academy of Sciences, Beijing 100190, China*

[2]*Beijing National Laboratory for Condensed Matter Physics, Institute of Physics, Chinese Academy of Sciences, Beijing 100190, China*

[3]*Key Laboratory for Optics, Beijing National Laboratory for Condensed Matter Physics, Institute of Physics, Chinese Academy of Sciences, Beijing 100190, China*

[4]*Technical Institute of Physics and Chemistry, Chinese Academy of Sciences, Beijing 100190, China*

(Received 20 July 2008; revised manuscript received 10 October 2008; published 19 November 2008)

High-resolution angle-resolved photoemission measurements have been carried out on the $(Sr,K)Fe_2As_2$ superconductor (T_c=21 K). Three holelike Fermi-surface sheets are resolved around the Γ point. One electronlike Fermi surface and strong Fermi spots are observed near the $M(\pi,\pi)$ point which are different from a round electron pocket expected from band calculations. This discrepancy and the observed band renormalization ask for further theoretical effort in understanding the electronic structure of the Fe-based compounds.

DOI: 10.1103/PhysRevB.78.184514 PACS number(s): 74.70.−b, 71.20.−b, 74.25.Jb, 79.60.−i

I. INTRODUCTION

The recent discovery of superconductivity in iron-based *R*FeAs(O,F) (*R* represents rare-earth elements such as La, Ce, Pr, Nd, Sm, etc.)[1–6] and $(A,K)Fe_2As_2$ (*A* represents alkaline-earth elements such as Ba and Sr)[7–10] has attracted great attention because they represent second class of high-temperature superconductors after the discovery of a first high-temperature superconductivity in cuprates.[11] Different from the cuprates where the parent compound is a Mott insulator,[12] the parent compounds of the iron-based superconductors show a metallic behavior with a spin-density wave (SDW) ground state.[13–15] This has raised an important question on whether one should treat iron-based compounds with an itinerant electron model[16,17] or localized correlated model.[18–21] Direct measurement of the electronic structure is crucial in addressing this issue, and particularly, the effect of electron correlation in this iron-based system.[22–24]

In this paper, we report first direct measurements of the Fermi surface and band structure of the $(Sr_{1-x}K_x)Fe_2As_2$ superconductor by angle-resolved photoemission (ARPES) measurements. We have clearly identified three holelike Fermi-surface sheets near the Γ point of the Brillouin zone, which is consistent with the band-structure calculations. We also observe an electronlike Fermi surface and strong Fermi spots near the $M(\pi,\pi)$ point. The overall electronic structure, particularly around the *M* point, shows significant difference from the band calculations of $BaFe_2As_2$. In addition, the observed bandwidth renormalization may suggest the importance of electron correlation in understanding the electronic structure of the iron-based compounds. These results provide important information in establishing the basic electronic structure of the iron-based high-temperature superconductors.

II. EXPERIMENTS

The angle-resolved photoemission measurements are carried out on our laboratory system equipped with a Scienta R4000 electron energy analyzer with a wide angle mode (30°).[25] We use a helium I resonance line as the light source which gives a photon energy of $h\nu$=21.218 eV. The light on the sample is partially polarized with the electric-field vector mainly in the plane of the sample surface [as shown in Fig. 1(b), bottom-left arrow]. The energy resolution was set at 12.5 meV and the angular resolution is ~0.3°. The Fermi level is referenced by measuring on the Fermi edge of clean polycrystalline gold that is electrically connected to the sample. The $(Sr_{1-x}K_x)Fe_2As_2$ single crystals were grown using the flux method,[26] and the crystal measured has a superconducting transition at T_c=21 K (onset) with a transition width of 3.5 K (10%–90% intensity standard), as shown from the magnetic measurement in Fig. 1(a). The precise K content in the $(Sr_{1-x}K_x)Fe_2As_2$ (T_c=21 K) is to be determined. From the known $T_c \sim x$ curve[8] relation it is estimated to be $x \sim 0.25$, so it is underdoped compared with optimal doping at x=0.4 with T_c=38 K. The crystal was cleaved *in situ* and measured in vacuum with a base pressure better than 6×10^{-11} Torr.

Figure 1 shows the Fermi surface [Fig. 1(b)], band structure [Figs. 1(c) and 1(d)], and corresponding photoemission spectra [energy distribution curves (EDCs)] [Fig. 1(e)] on $(Sr,K)Fe_2As_2$ single crystal around the Γ(0,0) point at a temperature of 45 K. The spectral weight distribution integrated over a narrow energy window [−5 meV, 5 meV] near the Fermi level [Fig. 1(b)] gives a good representation of the measured Fermi surface. Three Fermi-surface sheets can be clearly identified around the Γ point from Fig. 1(b), as marked in Fig. 3. The first is the well-defined inner small Fermi-surface sheet. The second is defined by nearly straight lines that can be clearly seen in Fig. 1(b). The third Fermi-surface sheet is defined by the outer strong intensity patches. We note that the overall spectral weight distribution is not symmetrical with fourfold symmetry with respect to the Γ point. This is due to the photoemission matrix element effect because the main electric-field component of the light is

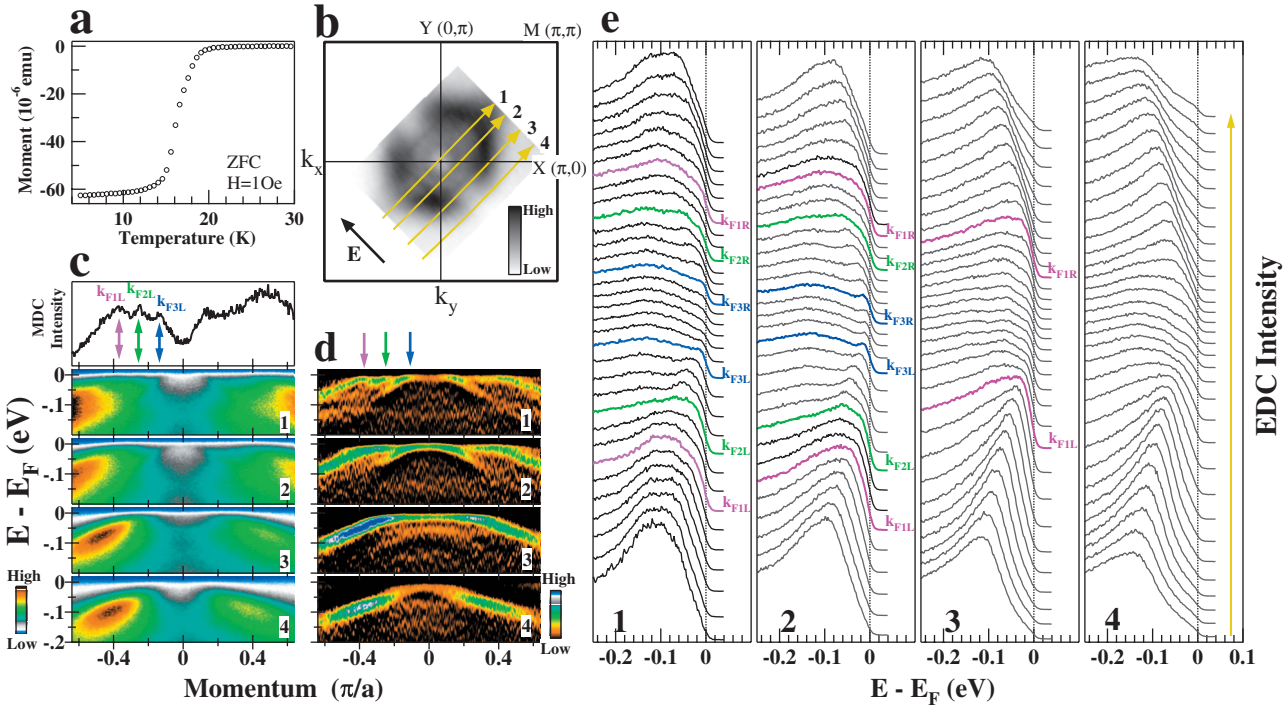

FIG. 1. (Color) Fermi surface, band structure, and photoemission spectra of $(Sr,K)Fe_2As_2$ (T_c=21 K) near the Γ point measured at 45 K. (a) Magnetic measurement of the superconducting transition temperature (T_c) of the single crystal under ARPES measurements (zero-field cooled, magnetic field H=1 Oe). (b) Spectral weight integrated within [−5 meV, 5 meV] energy window with respect to the Fermi level as a function of k_x and k_y. The black arrow near the bottom left marks the main electric-field direction on the sample surface from the light source. (c) Original photoemission images measured along the four typical cuts as marked in (a). The top panel shows the momentum distribution curve at the Fermi level for the photoemission image of cut 1. (d) Corresponding second derivative images of (c). (e) Photoemission spectra along the four cuts with EDCs at the Fermi momenta colored and marked.

along one particular diagonal direction as marked in Fig. 1(b).

Figure 1(c) shows photoemission data taken along several typical momentum cuts as marked in Fig. 1(b). The corresponding second derivative images, obtained by taking the second derivative on photoemission spectra with respect to the energy at each momentum, are shown in Fig. 1(d). This is an empirical but effective way in highlighting the underlying band structure.[27] From Figs. 1(c) and 1(d), three Fermi crossings can be seen, as marked by three arrows on the data for cut 1, which correspond to three Fermi-surface sheets near the Γ point. The Fermi momentum can be determined from the peak position in the momentum distribution curve (MDC) at the Fermi energy E_F, as shown in the top panel of Fig. 1(c). The measured bands further indicate that all of the three Fermi-surface sheets are holelike. These band dispersions and the Fermi crossings can also be seen from the corresponding photoemission spectra for the four cuts with the EDCs at the Fermi crossings marked by colored lines [Fig. 1(e)]. For the inner small Fermi sheet, clear EDC peaks are observed at the momentum crossings k_{F3L} and k_{F3R} in Fig. 1(e) for cuts 1 and 2. There is also a weak but visible flat band near −0.13 eV around the Γ point.

Figure 2 shows photoemission data of $(Sr,K)Fe_2As_2$ measured around the $M(\pi,\pi)$ point at 45 K. The spectral weight distribution [Fig. 2(a)] shows two strong intensity spots, S1 and S2, along the $\Gamma(0,0)$-$M(\pi,\pi)$-$(2\pi,2\pi)$ line, with their locations nearly symmetrical with respect to the $M(\pi,\pi)$ point. On both sides of the $\Gamma(0,0)$-$M(\pi,\pi)$-$(2\pi,2\pi)$ line, there are two patches of strong intensity. The maximum intensity contours on the two patches are not enclosed, and also, the two strong intensity spots appear to be isolated from the patches. These give rise to some disconnected Fermi crossings identifiable around the $M(\pi,\pi)$ point, as marked in Fig. 3. From the band-structure measurements [Figs. 2(b) and 2(c)], it is clear that the strong intensity spot, S1 in Fig. 2(a), originates from the band near the upper-left corner of Figs. 2(b) and 2(c) for cut 1. From Fig. 2(c), it is also clear that near the $M(\pi,\pi)$ point, the main electronic features are the two flat bands which are ~30 and ~80 meV below the Fermi level. The ~30 meV band crosses the Fermi level and forms an electronlike Fermi-surface sheet near the $M(\pi,\pi)$ point that corresponds to the contour of the maximum intensity contour of the two patches [as marked in Fig. 3(a) near the M point].

Figure 3 summarizes the overall Fermi surface of $(Sr,K)Fe_2As_2$ by combining both measurements around the Γ [Fig. 1(b)] and M points [Fig. 2(a)]. Three holelike Fermi-surface sheets are resolved around the Γ point, which are different from the two Fermi-surface sheets observed in $(Ba,K)Fe_2As_2$ compounds.[23,24] Interestingly, the shape of the three Fermi-surface sheets appears to be not circular but is more similar to squares. The enclosed area of the inner, middle, and outer Fermi sheets are ~0.06, ~0.28, and ~0.52, respectively, with a unit of $(\pi/a)^2$. On the other hand, for the M point, there is an electronlike Fermi-surface

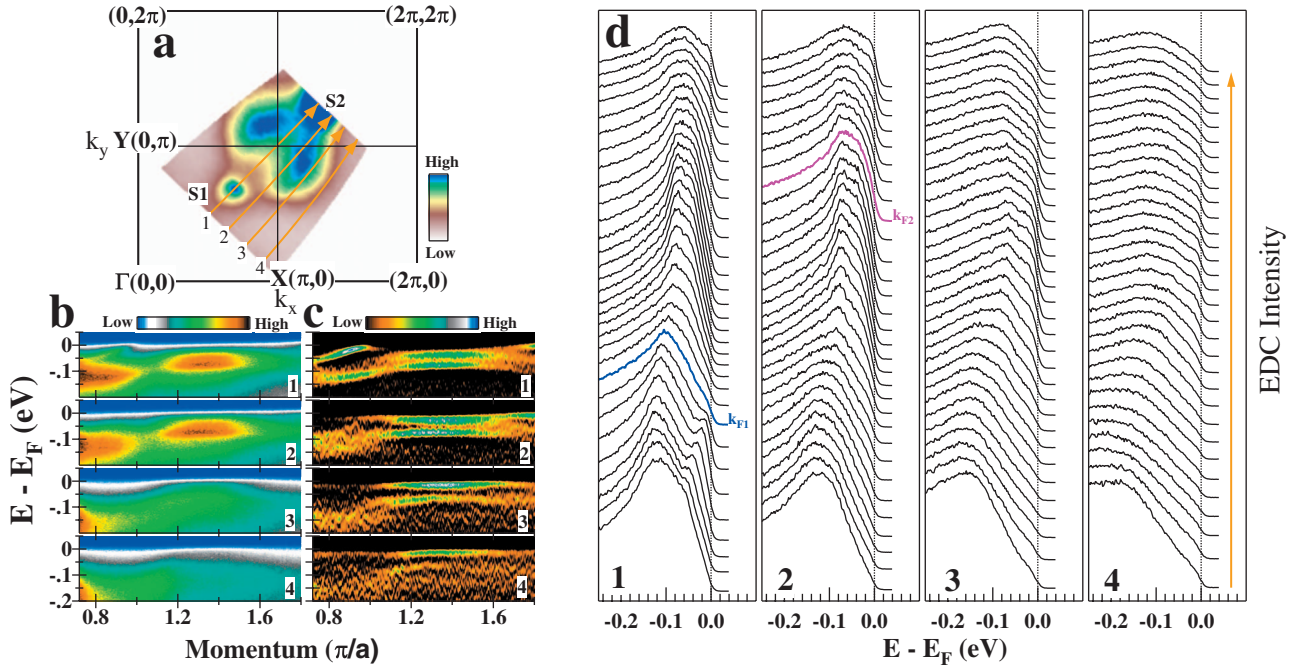

FIG. 2. (Color) Fermi surface, band structure, and photoemission spectra of $(Sr,K)Fe_2As_2$ near the $M(\pi,\pi)$ point. (a) Spectral weight distribution integrated within [−5 meV, 5 meV] energy window with respect to the Fermi level as a function of k_x and k_y. (b) Original photoemission images measured along the four typical cuts as marked in (a). (c) Corresponding second derivative images of (b). (d) Photoemission spectra along the four cuts with EDCs at the Fermi momenta colored and marked.

sheet associated with the Fermi crossings on the strong intensity patches [as marked near the M point in Fig. 3(a)]. However, because the patches are not enclosed near the M point, which is probably due to the matrix element effect and the appearance of two strong Fermi spots, S1 and S2, we need to further determine whether the two strong spots and the patches are independent or they belong to the same electronlike Fermi-surface sheet. Figures 3(b)–3(d) show spectral weight distribution integrated over different energy ranges away from the Fermi level. The strong Fermi spot S1 moves away from the M point with increasing binding energy, which is consistent with the band dispersion as seen from Figs. 3(b) and 3(c) (cut 1, upper-left band). On the other hand, the electronlike Fermi surface defined by the patches gradually shrinks toward the M point. This clearly indicates that the two strong Fermi spots, S1 and S2, are independent from the electronlike Fermi-surface sheet defined by the patches near the M point.

Figure 4 shows an overall band structure of $(Sr,K)Fe_2As_2$ along typical high-symmetry lines. This measurement, together with Fermi-surface information (Figs. 1–3), makes it possible to have a direct comparison with theoretical calculations. Since there are no band calculations available on $(Sr,K)Fe_2As_2$, we take the band calculations of $BaFe_2As_2$ (Refs. 24, 29, and 30) for comparison. This is reasonable because of the following two reasons: (1) according to the band calculation,[29] the band structure of $SrFe_2As_2$ is quite similar to $BaFe_2As_2$; and (2) band calculations on $(Ba_{1-x}K_x)Fe_2As_2$ indicate that upon potassium (K) doping in the parent compound $BaFe_2As_2$, the band structure basically follows a rigid-band shift.[24]

The observation of three holelike Fermi-surface sheets near the Γ point is consistent with the band calculations.[29] However, the overall measured band structure and Fermi surface show significant differences from the band calculated results,[24,29,30] particularly around the M point, in terms of the number, position, and shape of the bands. As shown in Fig. 4(c), four bands are expected from band calculations near the M point within the 0.6 eV energy range with two bands near −0.2 eV that give rise to two electronlike Fermi-surface sheets around the M point.[29] This is quite different from the experimental results where only two shallow flat bands are observed near ~−0.03 and ~−0.08 eV, and only one Fermi-surface sheet is identified. Moreover, the extra band along the Γ-M cut [Fig. 4(a)] that gives rise to the strong Fermi spots in the Fermi-surface mapping [Fig. 2(a)] is not present in the band calculation [Fig. 4(c)].

III. DISCUSSION

The deviation between the measured and calculated electronic structures may arise from a couple of reasons. First, although the band structure of $(Sr,K)Fe_2As_2$ is expected to be similar to that of $BaFe_2As_2$, it is desirable to compare the measured electronic structure with the calculated one on the same $(Sr,K)Fe_2As_2$ when it becomes available. In addition, there may be appreciable uncertainty in the band calculation itself. For instance, for the same $BaFe_2As_2$, the calculation by Liu *et al.*[24] gives only two Fermi crossings around the Γ point while three crossings are expected from calculations of other groups.[29,30] Second, there can be some uncertainty caused by k_z dispersion. For a given photon energy as we used, the measured electronic structure corresponds to one particular k_z with its location to be determined. However, we believe that this may not be the main reason because the

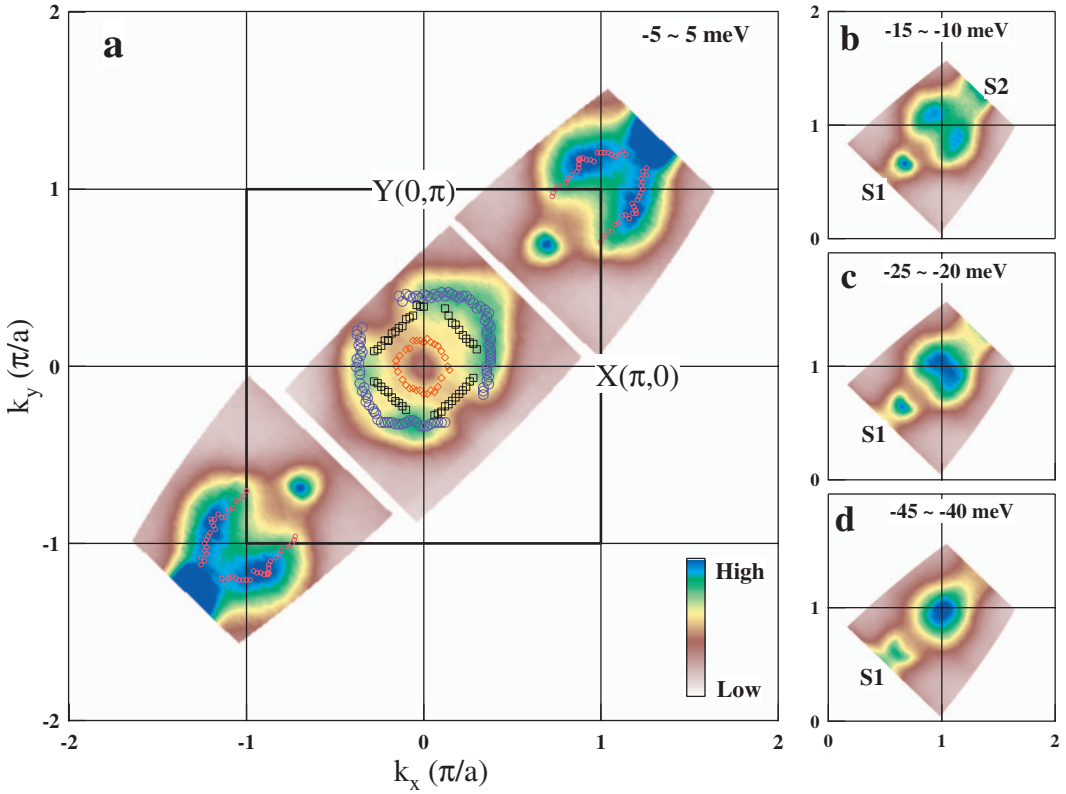

FIG. 3. (Color) Fermi surface of $(Sr,K)Fe_2As_2$. (a) Spectral weight distribution integrated over a small energy window [−5 meV, 5 meV] with respect to the Fermi level. The Fermi momenta are marked by symbols. (b)–(d) Spectral weight distribution near the $M(\pi,\pi)$ point integrated over energy windows of [−15 meV,−10 meV], [−25 meV,−20 meV], and [−45 meV,−40 meV], respectively, with respect to the Fermi level.

bands near the M point are not strongly sensitive to k_z.[29,30] Third, the effect of the SDW formation[15] on the electronic structure needs to be examined.[30] The two flat bands near the M point [Figs. 2(b) and 2(c)] are similar to those observed in the parent $BaFe_2As_2$ which may be related to the exchange splitting in the SDW state.[23] Fourth, the effect of the chemical-potential shift needs to be taken into account. The potassium (K^+) doping in the $(Sr,K)Fe_2As_2$ sample introduces holes and is expected to lower the chemical potential compared with the parent compound. Band calculations on $(Ba_{1-x}K_x)Fe_2As_2$ give a chemical-potential shift around 130 meV with x varying from 0 to 0.45.[24] For $(Sr_{1-x}K_x)Fe_2As_2$ with $x\sim0.25$, one may expect a chemical-potential shift of ~70 meV, compared with $x=0$. Putting the 70 meV chemical-potential shift downward into consideration, we find that the measured bands near the M point [Fig. 4(a)] are still hard to match with the calculated ones [Fig. 4(c)].[29] A better correspondence seems to be possible if one assumes a chemical-potential shift down by ~0.2 eV [as marked by a red dashed line in Fig. 4(c)]. In this case, there is one extra band along Γ-M which resembles the one in Fig. 4(a) that gives rise to strong Fermi spots in Fermi-surface mapping [Fig. 2(a)]. Near the M point, this would lead to two occupied bands with one band crossing the Fermi level to give an electronlike Fermi surface. The shift of the chemical potential to match the measured and calculated band structures is also proposed for another related compound LaFePO.[31] However, we note that while better agreement seems to be realized by such a chemical-potential shift in $(Sr,K)Fe_2As_2$, the physical origin of the shift is unclear. In addition, there remain quantitative discrepancies between the measured and calculated electronic structures in regard to the exact location of the Fermi crossings and quantitative bandwidth.

Another noticeable difference between the measurement and the band calculations is related to the width of the band dispersions. As seen from the calculated band structure [Fig. 4(c)], the major occupied bands along the Γ-M cut are spread up to the 0.6 eV energy range for $BaFe_2As_2$ while the observed bands are confined within 0.15 eV in the measured data [Fig. 4(a)]. We caution that because of the matrix element effect involved in the photoemission process, it is possible that some bands may be suppressed for one excitation photon energy. Also because the band structure near the M point is quite different from the band calculations, it is hard to make a clear correspondence between the measured and calculated bands which is desirable to examine the band renormalization effect. The three measured bands near the Γ point appear to have a better correspondence with the calculated three bands although it remains difficult to make an exact correspondence. However, among the three bands near the Γ point along the Γ-M cut in Fig. 4(a), two clear occupied bands show bottom near 0.06 and 0.14 eV in binding energy. These two bands, which are expected to belong to the group of the three calculated bands, are significantly narrower than the shallowest bands in the calculated band structure [Fig. 4(c)] where the bottoms of the three occupied

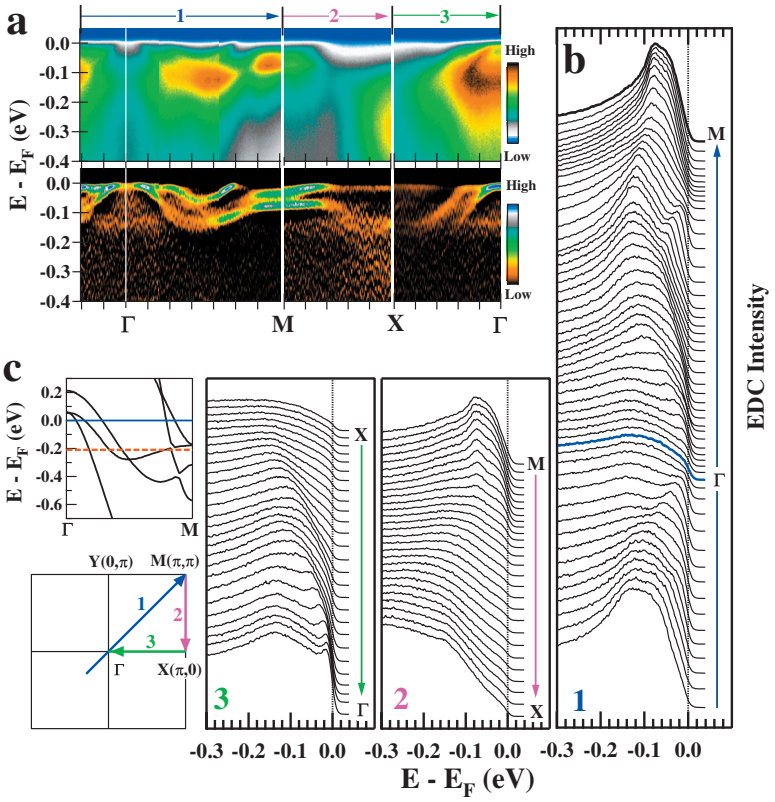

FIG. 4. (Color) Energy bands of $(Sr,K)Fe_2As_2$ along high-symmetry lines. (a) Original photoemission images (upper panels) and the corresponding second derivative images (lower panels) (Ref. 28). The locations of the momentum cuts are marked in the left-bottom inset. (b) Corresponding photoemission spectra. The corresponding momentum range is marked on top of (a). (c) Calculated band structure along the Γ-M direction in $BaFe_2As_2$ (Ref. 29).

bands near the Γ point are at 0.28, 0.44, and over 0.6 eV. The measured band narrowing remains even when a possible 0.2 eV chemical-potential shift downward is considered. This band renormalization effect suggests that electron correlation may play a role in describing the electron structure of the Fe-based compounds. A similar band renormalization effect is also reported in a related LaFePO compound near the Γ point.[31]

In summary, our angle-resolved photoemission measurements have provided detailed electronic structure of the $(Sr,K)Fe_2As_2$ superconductor. Significant deviation between the measured band structure on $(Sr,K)Fe_2As_2$ and calculated electronic structure on $BaFe_2As_2$ is revealed. The observed bands show obvious narrowing when compared with the calculated bandwidth of $BaFe_2As_2$. This information will ask for further theoretical efforts in understanding the electronic structure of the FeAs-based compounds.

ACKNOWLEDGMENTS

We thank Xiaogang Wen, Dunghai Lee, Zhong Fang, and Junren Shi for helpful discussions. This work was supported by the NSFC, the MOST of China (973 Projects No. 2006CB601002 and No. 2006CB921302), and the CAS (Projects ITSNEM).

*xjzhou@aphy.iphy.ac.cn

[1] Y. Kamihara, T. Watanabe, M. Hirano, and H. Hosono, J. Am. Chem. Soc. **130**, 3296 (2008).
[2] X. H. Chen, T. Wu, G. Wu, R. H. Liu, H. Chen, and D. F. Fang, Nature (London) **453**, 761 (2008).
[3] G. F. Chen, Z. Li, D. Wu, G. Li, W. Z. Hu, J. Dong, P. Zheng, J. L. Luo, and N. L. Wang, Phys. Rev. Lett. **100**, 247002 (2008).
[4] Z. A. Ren, J. Yang, W. Lu, W. Yi, X. L. Shen, Z. C. Li, G. C. Che, X. L. Dong, L. L. Sun, F. Zhou, and Z. X. Zhao, Europhys. Lett. **82**, 57002 (2008).
[5] Z. A. Ren, J. Yang, W. Lu, Wei Yi, G. C. Che, X. L. Dong, L. L. Sun, and Z. X. Zhao, Mater. Res. Innovations **12**, 105 (2008).
[6] Z. A. Ren, W. Lu, J. Yang, W. Yi, X. L. Shen, Z. C. Li, G. C. Che, X. L. Dong, L. L. Sun, F. Zhou, and Z. X. Zhao, Chin. Phys. Lett. **25**, 2215 (2008).
[7] M. Rotter, M. Tegel, and D. Johrendt, Phys. Rev. Lett. **101**, 107006 (2008).
[8] K. Sasmal, B. Lv, B. Lorenz, A. M. Guloy, F. Chen, Y.-Y. Xue, and C.-W. Chu, Phys. Rev. Lett. **101**, 107007 (2008).
[9] G. F. Chen, Z. Li, G. Li, W. Z. Hu, J. Dong, J. Zhou, X. D. Zhang, P. Zheng, N. L. Wang, and J. L. Luo, Chin. Phys. Lett. **25**, 3403 (2008).
[10] G. Wu, R. H. Liu, H. Chen, Y. J. Yan, T. Wu, Y. L. Xie, J. J. Ying, X. F. Wang, D. F. Fang, and X. H. Chen, Europhys. Lett. **84**, 27010 (2008).
[11] J. G. Bednorz and K. A. Müller, Z. Phys. B: Condens. Matter **64**, 189 (1986).
[12] P. A. Lee, N. Nagaosa, and X. G. Wen, Rev. Mod. Phys. **78**, 17 (2006).
[13] J. Dong, H. J. Zhang, G. Xu, Z. Li, G. Li, W. Z. Hu, D. Wu, G.

F. Chen, X. Dai, J. L. Luo, Z. Fang, and N. L. Wang, Europhys. Lett. **83**, 27006 (2008).
[14] Clarina de la Cruz, Q. Huang, J. W. Lynn, Jiying Li, W. Ratcliff, II, J. L. Zarestky, H. A. Mook, G. F. Chen, J. L. Luo, N. L. Wang, and Pengcheng Dai, Nature (London) **453**, 899 (2008).
[15] M. Rotter, M. Tegel, D. Johrendt, I. Schellenberg, W. Hermes, and R. Pöttgen, Phys. Rev. B **78**, 020503(R) (2008).
[16] D. J. Singh and M. H. Du, Phys. Rev. Lett. **100**, 237003 (2008).
[17] H. J. Zhang, G. Xu, X. Dai, and Z. Fang, arXiv:0803.4487 (unpublished).
[18] K. Haule, J. H. Shim, and G. Kotliar, Phys. Rev. Lett. **100**, 226402 (2008).
[19] C. Cao, P. J. Hirschfeld, and H. P. Cheng, Phys. Rev. B **77**, 220506(R) (2008).
[20] Z. P. Yin, S. Lebègue, M. J. Han, B. P. Neal, S. Y. Savrasov, and W. E. Pickett, Phys. Rev. Lett. **101**, 047001 (2008).
[21] F. J. Ma, Z. Y. Lu, and T. Xiang, arXiv:0804.3370 (unpublished).
[22] C. Liu, T. Kondo, M. E. Tillman, R. Gordon, G. D. Samolyuk, Y. Lee, C. Martin, J. L. McChesney, S. Bud'ko, M. A. Tanatar, E. Rotenberg, P. C. Canfield, R. Prozorov, B. N. Harmon, and A. Kaminski, arXiv:0806.2147 (unpublished).
[23] L. X. Yang, Y. Zhang, H. W. Ou, J. F. Zhao, D. W. Shen, B. Zhou, J. Wei, F. Chen, M. Xu, C. He, Y. Chen, Z. D. Wang, X. F. Wang, T. Wu, G. Wu, X. H. Chen, M. Arita, K. Shimada, M. Taniguchi, Z. Y. Lu, T. Xiang, and D. L. Feng, arXiv:0806.2627 (unpublished).
[24] C. Liu, G. D. Samolyuk, Y. Lee, N. Ni, T. Kondo, A. F. Santander-Syro, S. L. Bud'ko, J. L. McChesney, E. Rotenberg, T. Valla, A. V. Fedorov, P. C. Canfield, B. N. Harmon, and A. Kaminski, Phys. Rev. Lett. **101**, 177005 (2008).
[25] G. D. Liu, G. L. Wang, Y. Zhu, H. B. Zhang, G. C. Zhang, X. Y. Wang, Y. Zhou, W. T. Zhang, H. Y. Liu, L. Zhao, J. Q. Meng, X. L. Dong, C. T. Chen, Z. Y. Xu, and X. J. Zhou, Rev. Sci. Instrum. **79**, 023105 (2008).
[26] G. F. Chen, Z. Li, J. Dong, G. Li, W. Z. Hu, X. D. Zhang, X. H. Song, P. Zheng, N. L. Wang, and J. L. Luo, arXiv:0806.2648 (unpublished).
[27] W. T. Zhang, G. D. Liu, J. Q. Meng, L. Zhao, H. Y. Liu, X. L. Dong, W. Lu, J. S. Wen, Z. J. Xu, G. D. Gu, T. Sasagawa, G. L. Wang, Y. Zhu, H. B. Zhang, Y. Zhou, X. Y. Wang, Z. X. Zhao, C. T. Chen, Z. Y. Xu, and X. J. Zhou, Phys. Rev. Lett. **101**, 017002 (2008).
[28] The *X*-*M* measurement is obtained from the *Y*-*M* measurement which can be slightly different due to the matrix element effect from particular light polarization and sample measurement geometry.
[29] I. A. Nekrasov, Z. V. Pchelkina, and M. V. Sadovskii, JETP Lett. **88**, 144 (2008).
[30] F. J. Ma, Z. Y. Lu, and T. Xiang, arXiv:0806.3526 (unpublished).
[31] D. H. Lu, M. Yi, S.-K. Mo, A. S. Erickson, J. Analytis, J.-H. Chu, D. J. Singh, Z. Hussain, T. H. Geballe, I. R. Fisher, and Z.-X. Shen, Nature (London) **455**, 81 (2008).